Imaging standing surface plasmons by photon tunneling

A. Passian,[1,2,*] A. L. Lereu,[1,2,3] A. Wig,[1,2] F. Meriaudeau,[4] T. Thundat,[1,2] and T. L. Ferrell[1,2]
[1]*Oak Ridge National Laboratory, Oak Ridge, Tennessee 37831, USA*
[2]*Department of Physics and Astronomy, University of Tennessee, Knoxville, Tennessee 37996, USA*
[3]*Université de Bourgogne, Département de physique, 21011 Dijon, France*
[4]*Université de Bourgogne, IUT du Creusot, Le2i, 71200 Le Creusot, France*
(Received 11 December 2004; published 14 April 2005)

We present a direct method for optically exciting and imaging delocalized standing surface plasmons in thin metal films. We show theoretically that when imaging the field of the plasmons with a photon scanning tunneling microscope, the presence of the dielectric probe has a negligible effect on the surface modes of the metal film. We demonstrate that plasmon interference can be sustained in arbitrarily large regions of the metal film in comparison to the excitation wavelength. This knowledge can be important when seeking the relative distance between two scattering centers such as the presence of micron or submicron structures.

DOI: 10.1103/PhysRevB.71.165418 PACS number(s): 73.20.Mf, 42.25.Hz, 42.25.Kb, 68.37.−d

I. INTRODUCTION

Interference is by far one of the most intriguing phenomena of the submicron world. The holographic information carried by two interfering waves/particles—i.e., the amplitude and phase of the resulting field—has brought about many interesting applications in fields such as microscopy[1] and optical sensors.[2] In addition, surface modes of metals[3–5] have played a central role in scanning probe microscopy (SPM) and continue to be the subject of numerous recent studies.[6] An important category herein is the study of scattering and interference[7,8] of the surface plasmons[9,10] and how they may be probed.[11,12] We present in this paper a theoretical analysis, experimental observation, and imaging of standing-wave surface plasmons. These standing waves can be envisioned as the collective analog of electron holography and can open up new applications. In particular, due to the long coherence length of the standing waves, the potential of such phenomena for the detection of scattering centers can be used in single-molecule detection on smooth metal surfaces. However, the consequent spatially modulated electronic configurations need to be characterized. Such electronic modes and their associated periodicities may be studied by their surface electromagnetic fields. Reddick, Warmack, and Ferrell[13] showed that the signal generated in a photomultiplier tube by the action of photon tunneling from an evanescent field into a dielectric medium may provide a means of studying the topography, spectral characteristics, and electrodynamics of the hosting interface. However, the probing medium often interacts with the probed material in such a way that the surface modes and their resonance conditions may be modified.[14,15]

In this report, we study the influence of a dielectric probe on the surface plasmon dispersion relations of a thin metal film, which, owing to the relevant subwavelength dimensions involved, can be considered in the nonretarded limit. We thus begin Sec. II with the dispersion relations of the Kretschmann configuration,[16] followed by the analytical calculation and numerical evaluation of the new dispersion relations for the composite Kretschmann-probe system. The aim of our calculations is to provide qualitatively an estimate of the effect of the probe on the surface modes of metal substrate. In order to verify the experimentally observed interference pattern, due to two surface plasmons of opposite momenta, Sec. II ends with an analytical expression for the fringe separation. Having established the negligible distortion imposed by a dielectric probe, we, in Sec. III, using a photon scanning tunneling microscope, present and discuss the experimental observations in the near field of the standing surface plasmons, excited in a wide spectral range from the ultraviolet to infrared, as depicted schematically in Fig. 1. A conclusion is given in Sec. IV.

II. THEORETICAL DISCUSSIONS

We first note that the dispersion relation, for a dielectric (ϵ_t) bounded metal film (of thickness d) with a local dielectric function $\epsilon(\omega)$ residing on a dielectric substrate of dielectric function ϵ_s, can be calculated by solving the wave equation for the entire system and satisfying the boundary conditions on the fields $\mathbf{D}(\omega)=\epsilon(\omega)\mathbf{E}(\omega)$ at the charge-free $[\nabla\cdot\mathbf{E}(\omega)=0]$ interfaces, yielding

$$2k_2 d = \ln\left[\frac{[\epsilon_s k_2 - \epsilon(\omega)k_3][k_2\epsilon_t - k_1\epsilon(\omega)]}{[\epsilon_s k_2 + \epsilon(\omega)k_3][k_2\epsilon_t + k_1\epsilon(\omega)]}\right], \qquad (1)$$

which after some algebra can also be expressed as the following transcendental equation:

$$\epsilon^2(\omega) + \coth k_2 d\left(\frac{\epsilon_s}{k_3} + \frac{\epsilon_t}{k_1}\right)k_2\epsilon(\omega) + \epsilon_s\epsilon_t\frac{k_2^2}{k_1 k_3} = 0, \qquad (2)$$

where $k_i(\omega)=[\kappa^2-\epsilon_i(\omega)\omega^2/c^2]^{1/2}$, $i=1,2,3$, with $\epsilon_1=\epsilon_s$, $\epsilon_2=\epsilon(\omega)$, and $\epsilon_3=\epsilon_t$. For a vacuum-bounded foil, $\epsilon_t=1$. Assuming the upper surface of the metal resides at $z=0$, we next show how Eq. (2) is altered as a result of the presence of the dielectric probe in the subwavelength region of the metal surface. We take into account the finite curvature of the tip of the dielectric probe by modeling it as a single-sheeted hyperboloid of revolution in the prolate spheroidal coordinate system.[17] Using the Mehler-Fock integral transform,[18] we have derived a new infinite integral expansion[19] in order to

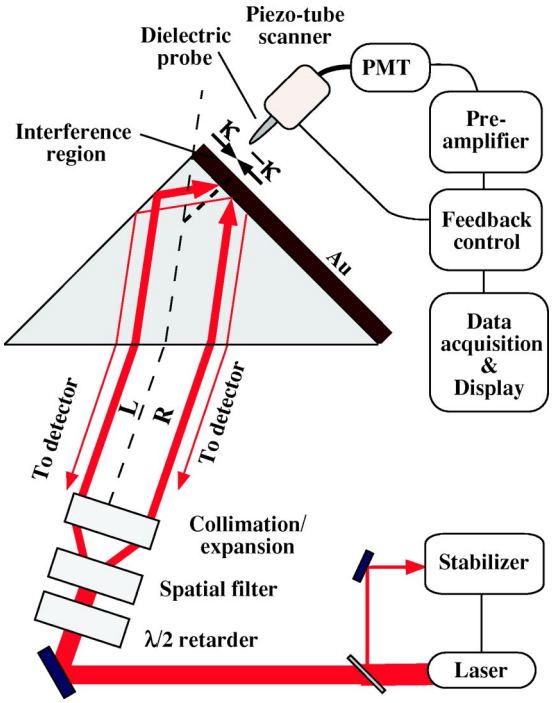

FIG. 1. Schematic representation of the experiment for imaging standing surface plasmons in the Kretschmann configuration using a photon scanning tunneling microscope. The left (L) and right (R) portions of the incident beam stimulate the same region of the film to excite two counterpropagating surface plasmons which will interfere to set up standing surface plasmons.

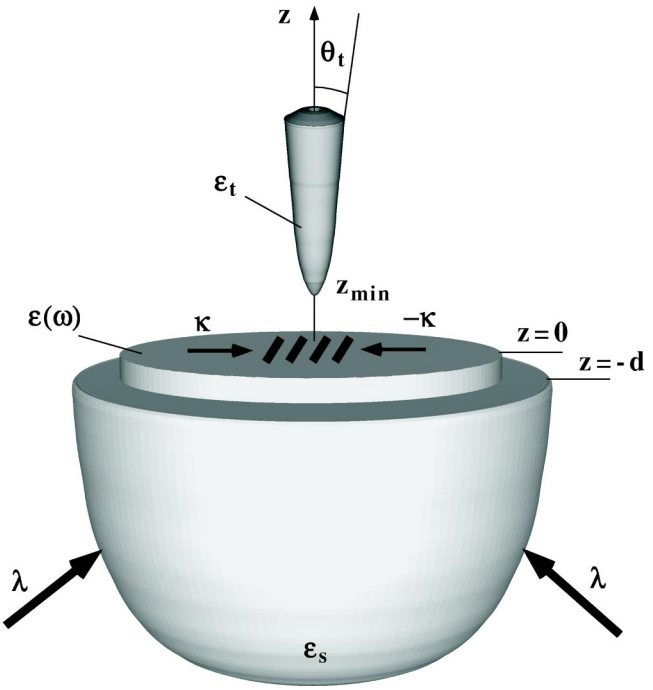

FIG. 2. Schematic representation of the probe-substrate geometry for imaging standing surface plasmons. The involved material domains are characterized by ϵ_t for the probe (here taken as quartz), $\epsilon(\omega)$ for the metal (here gold), and ϵ_s for the quartz substrate. The angle θ_t is the angle between the symmetry axis z and an asymptote to the probe. The upper surface of the film is defined by the plane $z=0$, while $z=-d$ defines the bottom plane. The counterpropagating plasmon wave vectors are denoted by $\pm\kappa$, while the excitation wave vector $k=2\pi/\lambda$.

satisfy the conventional Dirichlet-Neumann boundary conditions at the substrate surface. We thus show analytically, within the local dielectric theory, that the nonretarded modes of the thin metal-film substrate system are modified in such a way that the new modes are dictated by[19]

$$\epsilon^2(\omega) + \coth \kappa d[\epsilon_s + 1 + \mathcal{T}_q^m(\mu_t)]\epsilon(\omega) + \epsilon_s[1 + \mathcal{T}_q^m(\mu_t)] = 0, \tag{3}$$

where $\mathcal{T}_q^m(\mu_t)$ is defined as the tip influence function and is explicitly given by

$$\mathcal{T}_q^m(\mu_t) = 2\left(\frac{1}{\alpha_q^m(\mu_t)} - 1\right)^{-1}, \tag{4}$$

where

$$\alpha_q^m(\mu_t) = \left(\frac{\epsilon_t - 1}{\epsilon_t - \epsilon_q^m(\mu_t)}\right)\frac{P_{-1/2+iq}^m(\mu_t)}{P_{-1/2+iq}^m(-\mu_t)} \tag{5}$$

measures the polarizability of the probe and $\epsilon_q^m(\mu_t) = \epsilon_q^m(\mu)|_{\mu_t}$, with

$$\epsilon_q^m(\mu) = \frac{\partial_\mu P_{-1/2+iq}^m(\mu)}{\partial_\mu P_{-1/2+iq}^m(-\mu)}, \tag{6}$$

where ∂_μ partially differentiates the functions P with respect to the coordinate μ. The conical functions P can be represented by the hypergeometric functions for various ranges of its argument or by an integral representation.[20] The influence function $\mathcal{T}_q^m(\mu_t)$ has the limiting property that $\mathcal{T}_q^m(\mu_t) \to 0$ when $\epsilon_t \to 1$ corresponding to a reduction of Eq. (3) to the nonretarded limit of Eq. (2) [$k_i(\omega)=\kappa$, $i=1,2,3$, and $\epsilon_t=1.0$], that is,

$$\epsilon^2(\omega) + \coth \kappa d(\epsilon_s + 1)\epsilon(\omega) + \epsilon_s = 0, \tag{7}$$

in the absence of the probe. Here, the argument of the influence function is defined as $\mu_t = \cos\theta_t$, where θ_t is the angle between an asymptote to the probe hyperboloid and its axis of revolution ("tip angle," shown in Fig. 2), while for each surface plasmon mode κ, the superscript m corresponds to the discrete azimuthal eigenfunctions and the subscript q represents a continuous spectrum of the eigenvalues of the probe. Curve fitting to scanning electron microscope images of the probe provides the experimentally used numbers for θ_t in our work. The tip-film distance is defined by $z_{\min} = z_0 \cos\theta_t$, where z_0 is a scale factor. For $z_0 = 100$ nm and a probe angle $\theta_t = 46°$, the gap size is $z_{\min} = 69.5$ nm, which is in the near zone.

The influence function $\mathcal{T}_q^m(\mu_t)$, a complicated function of the conical functions,[21] is studied numerically to determine the influence of the probe as shown in Fig. 3. As can be seen from Fig. 3(a), only for small q values is there an observable influence [$\mathcal{T}_q^m(\mu_t) \neq 0$]. For $q=0$ (corresponding to large wavelengths), Fig. 3(b) displays $\mathcal{T}_0^m(\mu_t)$ as a function of the

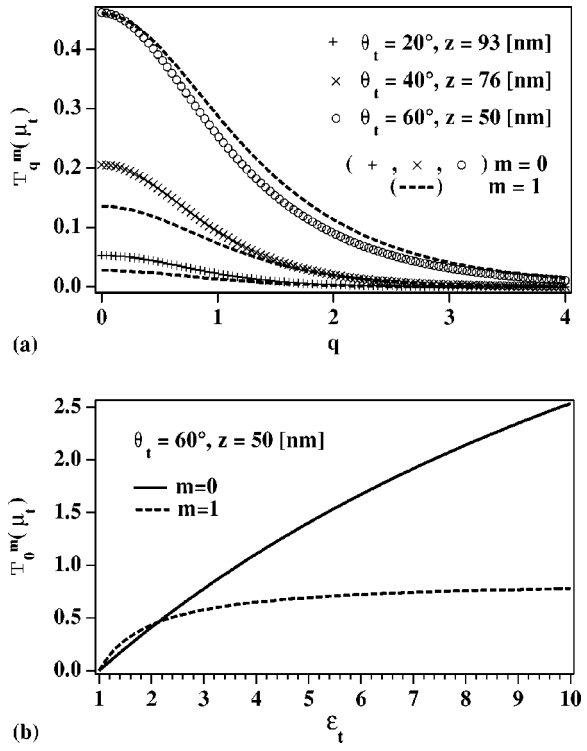

FIG. 3. The simulated behavior of the influence function, Eq. (4). (a) The higher the magnitude of $\mathcal{T}_q^m(\mu_t)$ for a probe defined by $\mu_t=\cos\theta_t$, the higher the extent to which the surface modes of the configuration in Fig. 2 deviate from those of an unperturbed foil. Noting that for a particular mode of the influence function represented by the pair (m,q), the closer to the surface and blunter the probe, the higher the magnitude above zero as expected. In the absence of the probe—that is, when $\epsilon_t=0$—then $\mathcal{T}_q^m(\mu_t)=0$ for all (m,q). This is particularly shown in (b) for the strongest modes [corresponding to $q=0$; see (a)], the effect being largest in the metallic tip limit $\epsilon\to\infty$.

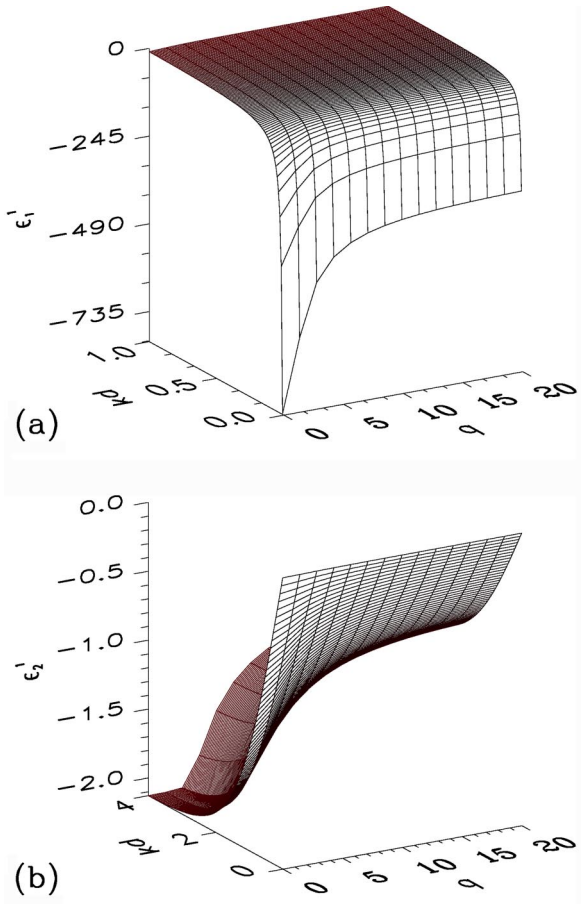

FIG. 4. The $m=1$ modification of the dispersion relation of a thin metal film on a dielectric half space corresponding to the symmetric (a) and antisymmetric (b) modes of the surface charge distribution. As can be seen for a fixed film thickness d, only a small momentum region experiences a negligible alteration, a behavior observed in all the roots of Eq. (3). The visible range 400–700 nm corresponds to the κd range (for a 45-nm-thick metal film) of 0.71–0.40.

dielectric constant of the dielectric probe medium. For $\epsilon_t=(1.46)^2=2.13$, corresponding to a quartz silicon multimode fiber used, we get $\mathcal{T}_0^m(\mu_t)<0.45$, whereas for large ϵ_t the influence increases so as to reach a maximum in the metallic tip limit. In this limit however, nanometer-sized probes do not represent a perfect conductor at optical frequencies, and plasmon excitations in the probe resulting in local (probe-geometry-dependent) field enhancement result in further complications of the dispersion relations of the system. This is further shown in Fig. 4 for the $(m=1)$ eigenmodes that satisfy Eq. (3). We note that in the nonretarded limit, Eq. (3) is no longer transcendental, and the lower indices 1 and 2 for $\epsilon_{1,2}^m$ in Fig. 4 label the two resulting solutions of Eq. (3). Alternatively, assuming a free electron model for the metal coating, the dispersion relations can be expressed as $\omega_{1,2}^m(q,\kappa d)=\omega_p[1-\epsilon_{1,2}^m(q,\kappa d)]^{-1/2}$, where ω_p denotes the plasma frequency.

In the limit of vanishing probe, the modes in Fig. 4(a) reduce to the symmetric modes of a thin foil on a dielectric substrate (given by $-\coth\kappa d/2$ for a vacuum bounded foil) and those in Fig. 4(b) to the antisymmetric modes (given by $-\tanh\kappa d/2$ for a vacuum bounded foil). We also note that the calculations presented here may be extended to include a study of the influence of a metal-coated dielectric probe on the surface modes of the Kretschmann configuration, a case for which optical access in the visible has been reported.[19,22] Through a comparison with the fully retarded Cartesian cases, we note that the inclusion of retardation has the effect of pushing the modes below the light line in the small momentum limit (for a fixed film thickness). These modes are however more photon like.[4]

Furthermore, with the metal surface defined by the $z=0$ plane, we can show that when the charge density $4\pi\rho(x,z,t)=\kappa\delta(z)\psi^0(z)\exp[i(\omega t-\kappa x+\pi/2)]$ associated with the excitation of the surface plasmons of wave vector κ encounters a counterpropagating charge oscillation of wave vector $-\kappa$, the resulting charge density will have a periodicity dictated by $\cos[(2k\sqrt{\epsilon_s}\sin\theta_{sp})x]$, so that the fringes are separated by $\Delta x=\pi/k\sqrt{\epsilon_s}\sin\theta_{sp}$, and are distributed along the interface at locations $x_m=m\Delta x$, $m=0,\pm1,\pm2,\ldots$. Here, k is the momentum of the excitation photons and θ_{sp} is the resonance angle.

III. EXPERIMENTAL RESULTS AND DISCUSSIONS

Our experimental arrangement is represented schematically in Figs. 1 and 2. The Kretschmann configuration is used to optically excite surface plasmons by directly evaporating a thin metal film onto a right-angled quartz prism. An expanded and spatially filtered incident laser beam is used to create the standing surface plasmons by internally splitting the laser beam by the prism itself, as shown in Fig. 1. This film-substrate system is then side mounted (vertical film plane) on a voltage-controlled rotation stage in order to accurately set the resonance angle. The photon scanning tunneling microscope (PSTM) scanner head (piezotube including the optical fiber probe) is also side mounted on the rotation stage such that the head and film plane can rotate with respect to the *p*-polarized incident laser beam. We have carried out the experimental measurements in the near field of the standing surface plasmons in the wavelength range from ultraviolet (325 nm) to infrared (1550 nm). For the ultraviolet to visible range, the tunneling signal is detected via a photomultiplier tube (Hamamatsu, with a spectral response in the range 185–850 nm and a peak response at $\lambda_p = 530$ nm, while a sensitive infrared detector module (Hamamatsu, InGaAs, noncooled-type, matched preamplifier, spectral response in the range 1.1–1.7 μm and a peak response at $\lambda_p = 1.55$ μm, sensitivity $= 10^6$ V/W at λ_p) is used for the infrared measurements at 1550 nm. By placing a microscope objective near the film surface, we have also observed the interference pattern in the far-field radiation originating from roughness induced scattering of surface plasmons. However, the aim of this work is to present a field pattern originating from the interference of surface plasmons in the near field.

Figure 5 displays the results for a 55-nm gold film excited with the $\lambda = 632.8$ nm line of a helium-neon laser (with an output power of 10 mW), incident at 46° with respect to the film's plane. Figure 6(a) represents the PSTM signal created by standing surface plasmons, excited on a 25-nm gold film with the $\lambda = 442$ nm line of a helium-cadmium laser, incident at 46.6° (Kimmon, 10 mW output power measured at the film plane). We note that the resonance angle, under these conditions, is 60°; however, the right-angled geometry does not allow the use of angles larger than 46.8°. This is due to the fact that the critical angle for the prism-air system is $\theta_c = 43.2°$, and thus any resonance angle (at the peak absorption) larger than $90.0° - 43.2° = 46.8°$ will couple out and the interference will not be installed. Nevertheless, because of the broad absorption band of the 442 nm excitation, we obtained the standing surface plasmons, as depicted in Fig. 6(a), by working off the peak absorption, which resulted in a weakening of the signal magnitude, but large enough to sense the pattern. We thus note that the results for this wavelength can be improved by the use of a spectrally optimized film thickness (24 nm for Au, and 45 nm for Ag), in a different arrangement, where the two interfering beams are delivered independently as in the case of classical holography, without the aforementioned angular limitation. Figure 6(b) displays the standing surface plasmons stimulated by the $\lambda = 1550$ nm line of a continuous-wave laser (Streamline-RL, Spectra-Physics, with an output power of <100 mW measured at the film plane), incident at 46° at a 29.5-nm gold film. Prior to each measurement, an exponentially decaying surface plasmon field is detected and examined. For the case of Fig. 5, the normalized tunneling current can accurately be

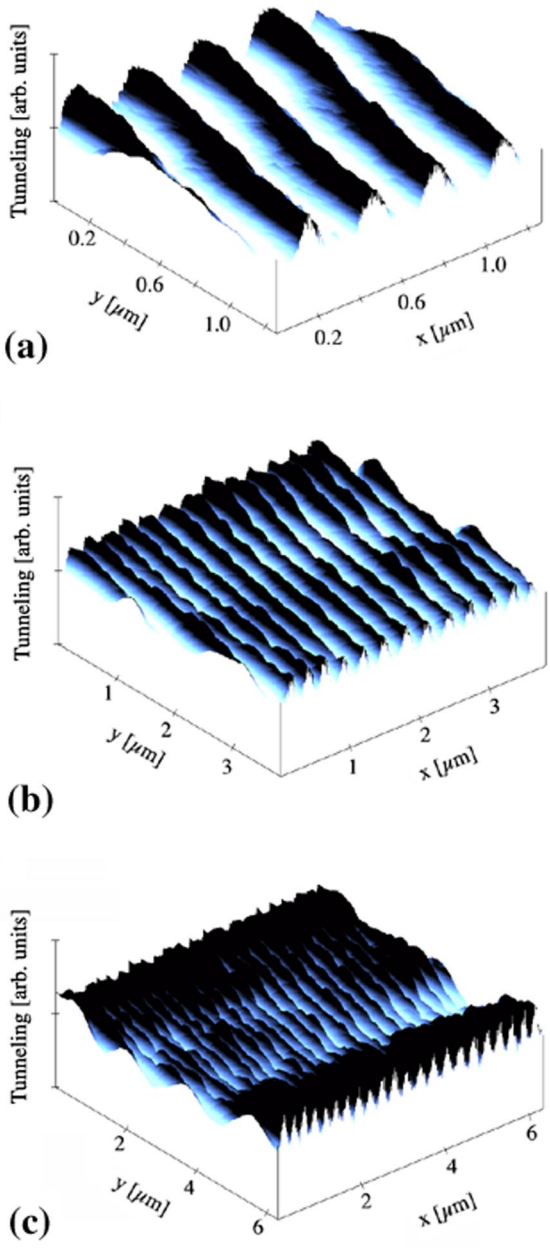

FIG. 5. Standing surface plasmons excited at $\lambda = 632.8$ nm on a 55-nm gold foil is sensed by the probe of a photon scanning tunneling microscope. When imaging the field of the plasmons, the presence of the dielectric probe has negligible effect on the modes of the metal film and plasmon interference can be sustained in arbitrarily large regions in comparison with the excitation wavelength. The formation of the interference pattern due to the standing surface plasmons in the metal film is further supported by a decrease in the intensity of the fringes upon (1) a continuous variation of the polarization state of the incident field from $p \rightarrow s$, (2) an inhibition of either L or R beam, and (3) a shift away from resonance of the angular or spectral position of the excitation beam. No image processing was performed on the presented data.

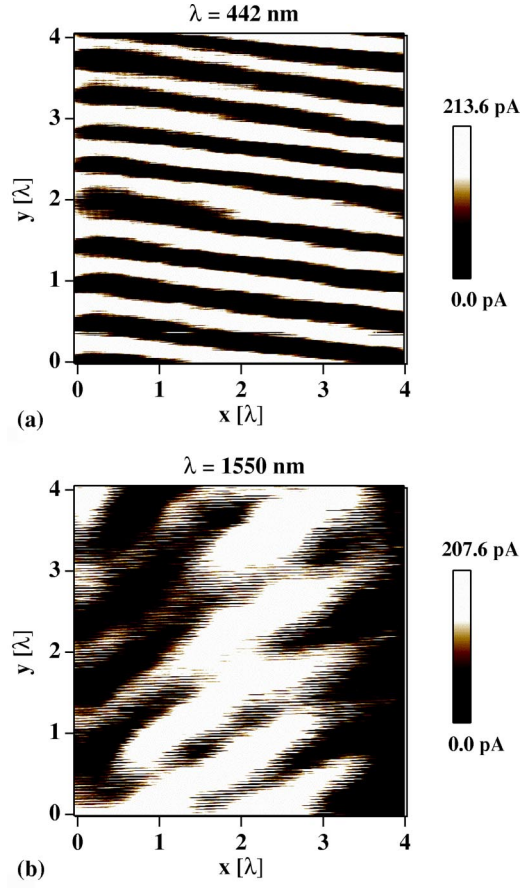

FIG. 6. Photon scanning tunneling microscope images of standing surface plasmons over a $4\lambda \times 4\lambda$ region, excited, respectively, at (a) $\lambda = 442$ nm using a 25-nm gold film and (b) $\lambda = 1550$ nm using a 29.5-nm gold film. The scale bars indicate the relative range of the amplitude of in the detected signal.

described by $f(z) = a + b\exp(-cz)$, where $a = 0.0909 \pm 0.0002$, $b = 0.9240 \pm 0.0006$, and $c = 0.012962 \pm 1.63 \times 10^{-5}$, for a relative initial distance to the foil surface. Such exponential behavior is clearly absent in the case of scattered fields. The fast Fourier transform (FFT) of the images presented no other periodicities in the data displayed in Figs. 5 and 6. For clarity, this is shown in Fig. 7(a) for a direction parallel to the x component of the surface plasmon wave vector and is reinforced by the power spectral density along a line perpendicular to the fringes displayed in Fig. 7(b), for the 632.8 nm wavelength. A fringe separation of $\Delta x = 302$ nm can be obtained from the fast Fourier transform analysis of the $n\lambda \times n\lambda$ images with n up to 15. For the parameters of our experiment, the predicted fringe separation (from Sec. I) is $\Delta x = 301.3$ nm, which is in good agreement with the experimental value. The observed images can be described by the function $\cos(x,y)$, with a similar response (double spike) in their Fourier space. No fringes can be observed if the polarization state of the plasmon excitation beam is changed from p to s, a portion of the excitation laser beam is inhibited, or if the resonance characteristics (angular or spectral position) are shifted. No image processing was performed on the presented images. For example, low-pass filtering of the images will readily remove the scan lines presented in all the images.

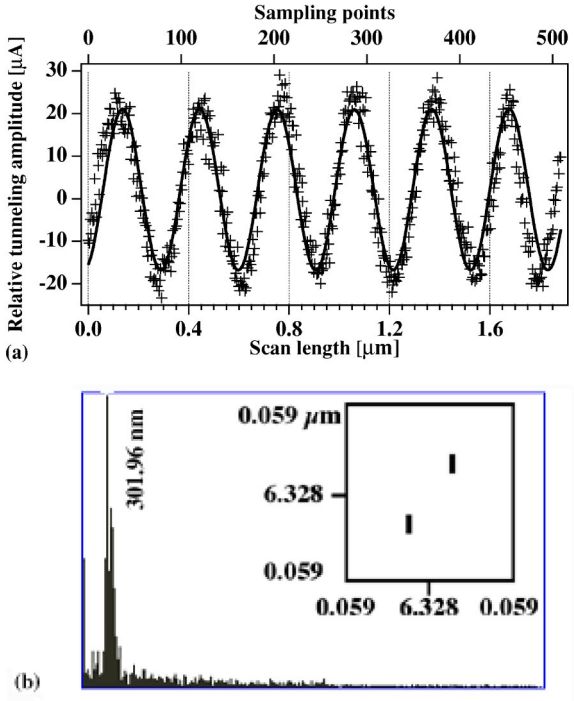

FIG. 7. (a) A line profile (symbols) in the direction parallel to the plasmon wave vector κ_x. The fitted function $u(x) = 2.1 - 18.9\cos(20.4x + 0.3)$ (solid curve) yields a period of 0.3 μm. We note that this tunneling signal, detected by the probe and photomultiplier combination, is a direct consequence of the plasmon field amplitudes. In particular, we note the difference of this signal from the traditional PSTM signal, where the tunneling photons are provided by the evanescent field produced by total internal reflection at the sample/substrate interface. (b) Power spectral density along a line perpendicular to the fringes. The inset shows the two-dimensional FFT spectrum of the image in Fig. 5. The off-vertical axis placement of the spikes is a result of the small angle of the fringes with respect to the horizontal axis in image of Fig. 5.

IV. CONCLUSIONS

We have investigated the generation and imaging of large-area standing surface plasmons in thin metal films in a straightforward arrangement. We conclude from the behavior of the nonretarded dispersion relations for the surface plasmons in the probe-metal system that the energy of the surface plasmon "grating" is negligibly altered by the approaching dielectric probe. From our results we conclude that plasmon interference can be sustained in an arbitrarily large region in comparison to the excitation wavelength. This knowledge can be important when evaluating the smoothness of the film surface or when seeking the relative distance between two scattering centers such as the presence of micron or submicron structures. The far-field radiation intensity of the interference pattern due to scattering yields a measure of the surface roughness. If one of the (κ or $-\kappa$) plasmons or both scatter inelastically before or during interference on a

smooth foil, then it is conceivable that a void or a distortion will appear in the near-field pattern shown in Figs. 5 and 6. Such spatially modulated giant field magnitudes can be useful in surface enhanced Raman scattering (SERS). The relatively simple experimental configuration can be appropriate for surface plasmon holography and lithography, where a photoactive material on the surface of the metal film can record the pattern. Surface plasmons with wavelengths smaller than the exciting light and multiple wavelength excitations may be used to create a grating with variable periodicity, an application in optical signal processing. Important advances in these areas may be possible if the direction of the surface plasmons grating can be altered or modulated. Access to the film surface may be useful for sensing applications, scanning probe microscopy, and nanotechnology research. Variations in physical quantities such as temperature, volume, and elasticity that cause either of the two interfering beams to vary in phase or amplitude may be detected using the method described.

ACKNOWLEDGMENTS

This work was supported by the DOE BES. Oak Ridge National Laboratory, Oak Ridge, Tennessee, 37831-6123, is managed by UT-Battelle, LLC for the Department of Energy under Contract No. DE-AC05-0096OR22725.

*Electronic address: passianan@ornl.gov

[1] S. Amelinckx, D. van Dyck, J. van Landuyt, and G. van Tendeloo, *Handbook of Microscopy* (Wiley-VCH, Berlin, 1997).
[2] W. Göpel, J. Hesse, and J. N. Zemel, *Sensors* (Wiley, New York, 1997).
[3] A. Liebsch, *Electronic Excitations at Metal Surfaces* (Plenum, New York, 1997).
[4] B. E. Sernelius, *Surface Modes in Physics* (Wiley-VCH, Berlin, 2001).
[5] A. D. Boardman, *Electromagnetic Surface Modes* (Wiley, New York, 1982).
[6] S. Kawata, *Near Field Optics and Surface Plasmon Polaritons* (Springer, New York, 2001).
[7] B. Hecht, H. Bielefeldt, L. Novotny, Y. Inouye, and D. W. Pohl, Phys. Rev. Lett. **77**, 1889 (1996).
[8] L. Novotny, B. Hecht, and D. W. Pohl, J. Appl. Phys. **81**, 1798 (1996).
[9] R. H. Ritchie, Phys. Rev. **106**, 874 (1957).
[10] T. L. Ferrell, T. A. Callcott, and R. J. Warmack, Am. Sci. **73**, 344 (1985).
[11] P. Dawson, F. de Fornel, and J.-P. Goudonnet, J. Appl. Phys. **81**, 1798 (1996).
[12] M. Specht, J. D. Pedarnig, W. M. Heckl, and T. W. Hänsch, Phys. Rev. Lett. **68**, 476 (1992).
[13] R. C. Reddick, R. J. Warmack, and T. L. Ferrell, Phys. Rev. B **39**, 767 (1989).
[14] T. L. Ferrell, Phys. Rev. B **50**, 14 738 (1994).
[15] T. L. Ferrell, Nucl. Instrum. Methods Phys. Res. B **96**, 483 (1995).
[16] E. Kretschmann, Z. Phys. **241**, 313 (1971).
[17] N. N. Lebedev, *Special Functions and Their Applications* (Dover, New York, 1972).
[18] B. N. Mandal and N. Mandal, *Integral Expansions Related to Mehler-Fock Type Transforms* (Longman, London, 1997).
[19] A. Passian, R. H. Ritchie, A. L. Lereu, T. Thundat, and T. L. Ferrell, Phys. Rev. B **71**, 115425 (2005).
[20] I. N. Sneddon, *The Use of Integral Transform* (McGraw-Hill, New York, 1972).
[21] K. S. Kölbig, Comput. Phys. Commun. **23**, 51 (1981).
[22] A. Passian, A. Wig, A. L. Lereu, F. Meriaudeau, T. Thundat, and T. L. Ferrell, Appl. Phys. Lett. **85**, 3420 (2004).